DTM Generation from Ikonos In-Track Stereo Images Using a 3D Physical Model♥

Thierry Toutin
Canada Centre for Remote Sensing, Natural Resources Canada
588, Booth Street, Ottawa, Ontario K1A 0Y7

ABSTRACT

A digital elevation model (DEM) extracted from Ikonos in-track stereo images using a 3D physical model developed at the Canada Centre for Remote Sensing, Natural Resources Canada was evaluated. First, the stereo photogrammetric bundle adjustment was set up with about ten accurate ground control points. The DEM was then generated using an area-based multiscale image matching method and 3D semiautomatic editing tools and then compared to lidar elevation data with a 0.2-m accuracy. Because the DEM is, in fact, a digital terrain surface model where the height of land covers (trees, houses) is included, the accuracy varies depending on the land cover types. Using 3D visual classification of the stereo Ikonos images, different classes (forests, residential, bare soil, lakes) were generated to take into account the height of the surface (natural and human-made) in the accuracy evaluation. An elevation linear error with 68 percent confidence level (LE68) of 1.5 m was obtained for bare surfaces while an LE68 of 6.4 m was achieved over the full area. Five-meter contour lines could thus be derived, compliant with the highest topographic standard. Better results could be thus expected when using stereo-images acquired in summertime. On the other hand, an LE68 of 2.5 m to 6.6 m were obtained depending on the land-cover type and its surface height. For residential areas, the surface height did not affect the errors very much (2.5-m LE68) when compared to bare surface results because one- and two-story houses were sparse in the test area. Because the images were unfortunately acquired in wintertime and the lidar data in summertime, elevation errors (LE68 and bias) also depended on the type of forests (deciduous, coniferous, mixed, sparse). An evaluation based on terrain slope and azimuth showed that the DEM error was linearly correlated with slope and that the elevations on sun-facing slopes were 1-m more accurate than elevations on slopes facing away from the sun.

1 INTRODUCTION

The generation of high-resolution imagery using previously proven defense technology provides an interesting source of data for digital topographic mapping as well as thematic applications such as agriculture, forestry, and emergency response (Kaufmann und Sulzer, 1997; Konecny, 2000). Technical information regarding the new U.S. civilian satellites with their applicability to Earth sciences have been summarized by

♥ Published in Photogrammetric Engineering & Remote Sensing 70(6):695-702, June 2004

Fritz (1996). Ikonos, successfully launched on 24 September 1999 (www.spaceimaging.com) was the first civilian satellite with these new high-resolution sensors (1-m panchromatic, Pan and 4-m multiband, XS) and an off-nadir viewing capability (up to 60º in any azimuth). This 360º pointing capability enables the generation of across-track stereoscopic images from two different orbits, such as with SPOT-HRV, as well as of in-track stereoscopic images from the same orbit, such as with JERS-1's Optical Sensor with base-to-height ratio (B/H) of one. Users could then apply traditional 3D photogrammetric techniques with the stereo images to extract accurate planimetric and elevation information. In fact, same-date in-track stereo data acquisition gives a strong advantage over multidate across-track stereo data acquisition because it reduces radiometric image variations (temporal changes, sun illumination, etc.), and thus increases the correlation success rate in any image matching process (Toutin, 2000). This in-track solution to acquiring stereo data is generally chosen by Space Imaging not only for scientific, but also for operational reasons.

Due to high spatial resolution of recent airborne/spaceborne sensors in the visible and microwave spectrum, a large number of researchers around the world have investigated the extraction of elevation and/or the production of DEMs using different methods (Leberl, 1998; Madsen and Zebker, 1998; Toutin, 2000). In preparation for the launch of high-resolution civilian satellites, Ridley *et al.* (1997), using similar systems mounted on aircraft platforms or from scanned aerial photos, demonstrated that Ikonos stereo images should have a potential for creating DEMs with about a 2-m accuracy, but only if photogrammetric processing is employed (Li, 1998). After the launch of Ikonos, some preliminary evaluations on 3D point positioning or feature extraction, using manual/visual processes, were addressed (Tao and Hu, 2002; Fraser *et al.*, 2002). On the other hand, Toutin *et al.* (2001) and Muller *et al.* (2001) generated a full DEM from Ikonos in-track stereo images using an automatic process. The objectives of this paper are to expand on these preliminary results using photogrammetric-based multisensor 3D geometric modeling developed at the Canada Centre for Remote Sensing (CCRS) (Toutin, 1995) and adapted to Ikonos images (Toutin and Cheng, 2001; Toutin, 2003). The paper evaluated DEM quality when compared to accurate ground truth, and tracked the error propagation from the input data to the final DEM. Different parameters affecting the accuracy were also evaluated.

2 DESCRIPTION OF THE METHOD

Ikonos Stereo Data and Study Site

Ikonos stereo images are only distributed in a quasi epipolar-geometry reference where just the elevation parallax in the scanner direction remains (www.spaceimaging.com). For in-track stereoscopic image capture with the Ikonos orbit inclination, the image orientation approximately corresponds to a north-south direction, with few degrees in

azimuth depending on the across-track component of the total collection angle (Figure 1).

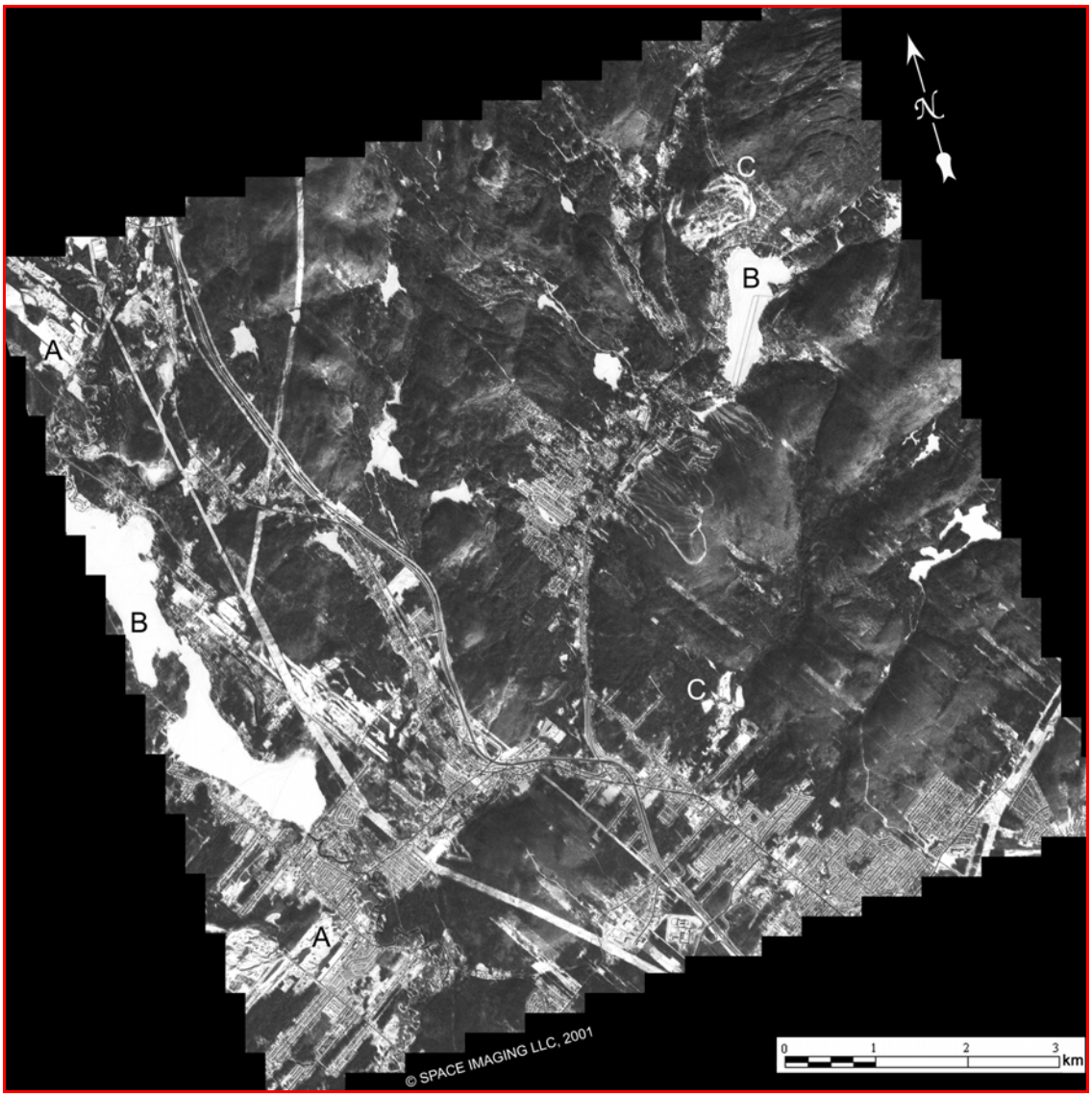

Figure 1. Backward sub-image mosaic Ikonos, north of Québec City, Quebec, Canada acquired 03 January 2001. Note (A) sand/gravel pits, (B) frozen lakes with snow, and (C) snow over bare soil. Ikonos Image © Space Imaging LLC, 2001.

The Ikonos stereo product was requested in autumn 2000 for an area north of Québec City, Québec, Canada (N 47º, W 71º 30'). This study is a residential and semirural environment and has a hilly topography with a 450-m elevation range. Unfortunately, the ±27° in-track stereo images (10 km by 10 km; B/H of one) with 252° and 322° azimuths were acquired on 03 January 2001 when the sun illumination angle was as low

as 19º, resulting in long shadows. In addition, each image was subdivided in two sub-images generating two stereo-pairs (West and East) with a B/H of one, and had to be processed separately. Figure 1 is the backward sub-image mosaic (just for display purpose): one can notice sand/gravel pits (A), frozen lakes with snow (B), and snow over bare soil (C). Figure 2 is an enlargement, which shows the tree shadow on the lake (A) and the mountain shadow (B) due to the 19º solar illumination angle.

Figure 2. Sub-image of backward image of the Ikonos stereo pair, north of Québec City, Quebec, Canada. Note (A) tree shadows and (B) mountain shadows due to a 19° solar elevation angle and 166° azimuth angle and (C) a skater.
Ikonos Image © Space Imaging LLC, 2001.

Fifty-five GCPs —25 and 30 on the West and East sub-images, respectively— were collected stereoscopically for the different tests of the bundle adjustment using the stereoscopic pair. Their cartographic coordinates (*X*, Y, *Z*) were stereo-compiled by the *Ministère des Ressources naturelles du Québec*, Canada from aero-triangulated 1:40,000-scale photographs using a Wild A-10. The accuracy is estimated to be better than 1 m and 2 m in planimetry and elevation, respectively. A topographic DEM with a 5-m grid spacing and 5-m elevation accuracy was also available from the same *Ministère*. Because the topographic DEM was not accurate enough, it was only used to derive a digital terrain slope model (DTSM) with the same pixel spacing. Figure 3 is the histogram of the DTSM. The bin of 0° slope represents 25 percent of the total slopes, where 5 percent are lakes. The mean slope is 6 to 7°, and the bins of 0 to 25° slopes represent 99 percent of total slopes. At slopes over 18°, each bin represents less than 1 percent of total slopes, and slopes greater than 30° represent only 0.24 percent of total slopes.

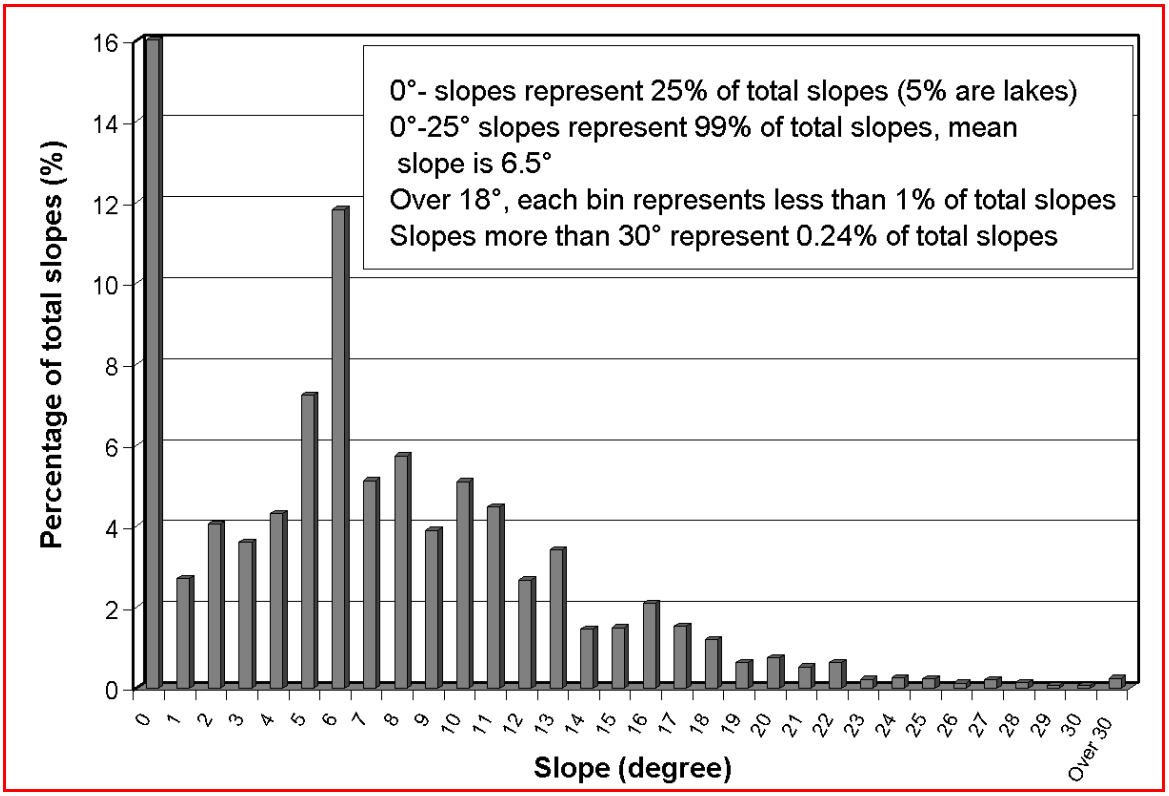

Figure 3. Histogram of the digital terrain slope model (DTSM) with 1° bin. The mean slope is 6-7°. Slopes greater than 30° are grouped because they represent only 0.24 percent of total slopes.

In addition, accurate spot elevation data was obtained on 06 September 2001 from a lidar survey by GPR Consultants (www.lasermap.com). The Optech ALTM-1020 system is comprised of a high frequency optical laser coupled with Global Positioning System (GPS) and an inertial navigation system (INS) (www.optech.on.ca). A 3D GPS solution (*X*, *Y*, *Z*) is used to position the laser scanner at each second or half second, while the INS data are used to determine the systems' orientation. The GPS solution is computed from differential kinematic processing using data collected simultaneously at the aircraft and at base stations near the project site (Fowler, 2001). From a fixed-wing airborne platform, the laser emits pulses at frequencies of up to 5000 Hertz and the first-echo pulses are reflected off vegetation or man-made structures and recorded. With 700- to 850-m flying height, 70-m/s velocity, 5000 Hertz pulse rate, 12 Hertz scanning frequency, and ±20° scan angle (510- to 630-m-wide swath), the ground point density was about 300,000 3D points per minute and the accuracy was 0.30 m in planimetry and 0.15 m in elevation. Ten swaths were acquired covering an area of 5 km by 11 km, which approximately corresponds to the East stereo pair. The results are then an irregular-spaced grid (around 3 m), due also to no echo return in some conditions (buildings with black roof, some roads, and lakes). Because the objectives were to evaluate the stereo Ikonos DEM, the lidar elevation data was not interpolated into a regular-spaced grid to avoid the propagation of interpolation error into the checked elevation and the evaluation.

The 3D CCRS Physical Model

The 3D CCRS physical model was originally developed to suit the geometry of pushbroom scanners, such as SPOT-HRV, and was subsequently adapted as an integrated and unified geometric modeling to geometrically process multisensor images (Toutin, 1995). This 3D physical model applied to different image types is robust and not sensitive to GCP distribution when there is no extrapolation in planimetry and elevation. The geometric modeling represents the well-known collinearity condition (and coplanarity condition for stereo model), and takes into account the different distortions relative to the global geometry of viewing: i.e.,

- the distortions relative to the platform (position, velocity, orientation),
- the distortions relative to the sensor (orientation angles, instantaneous field of view, detection signal integration time),
- the distortions relative to the Earth (geoid-ellipsoid, including elevation), and
- the deformations relative to the cartographic projection (ellipsoid-cartographic plane).

More recently, the model has been adapted to Ikonos images by taking into account the image characteristics and the available information in the metadata file (Toutin and Cheng, 2001). More details on the mathematic model and development (colinearity equations), its applicability and full results with a large data set of Ikonos images and

cartographic data acquired around the world can be found in Toutin (2003).

The Processing Steps for DEM Generation

Because the processing steps of DEM generation from Ikonos stereo images are roughly the same as for other stereo images (data collection and preprocessing, stereo bundle adjustment with GCPs, elevation parallax measurements, DEM generation and editing), the six processing steps (Figure 4) are only summarized (Toutin, 1995):

1. Acquisition and preprocessing of the remote sensing data (images and metadata) to determine an approximate value for each parameter of 3D physical model for the two images;

2. Collection of GCPs with their 3D cartographic coordinates and 2D image coordinates, the GCPs covering the total surface with points at the lowest and highest elevation to avoid extrapolations, both in planimetry and elevation. The image pointing accuracy was generally one pixel but sometimes two pixels.

3. Computation of the 3D stereo model, initialized with the approximate parameter values and refined by an iterative least-squares bundle adjustment with the GCPs (Step 2). Both equations of colinearity and coplanarity are used as observation equations and weighted as a function of input errors. Theoretically six accurate GCPs are enough to compute the stereo model, but more GCPs were acquired in order to provide an overestimation in the adjustment, reducing the impact of errors or to perform accuracy tests with independent check points (ICPs).

4. Extraction of elevation parallaxes using multiscale mean normalized cross-correlation method with computation of the maximum of the correlation coefficient. This method gave good results and was commonly used with satellite images (Gülch, 1991);

5. Computation of *XYZ* cartographic coordinates from elevation parallaxes (Step 4) using the previously computed stereo model (Step 3) with a 3D least-squares stereo intersection; and

6. Generation of regular grid spacing with 3D automatic and 3D visual editing tools: automatic for blunders removal and for filling the small mismatched areas and visual for filling the large mismatched areas and for the lakes.

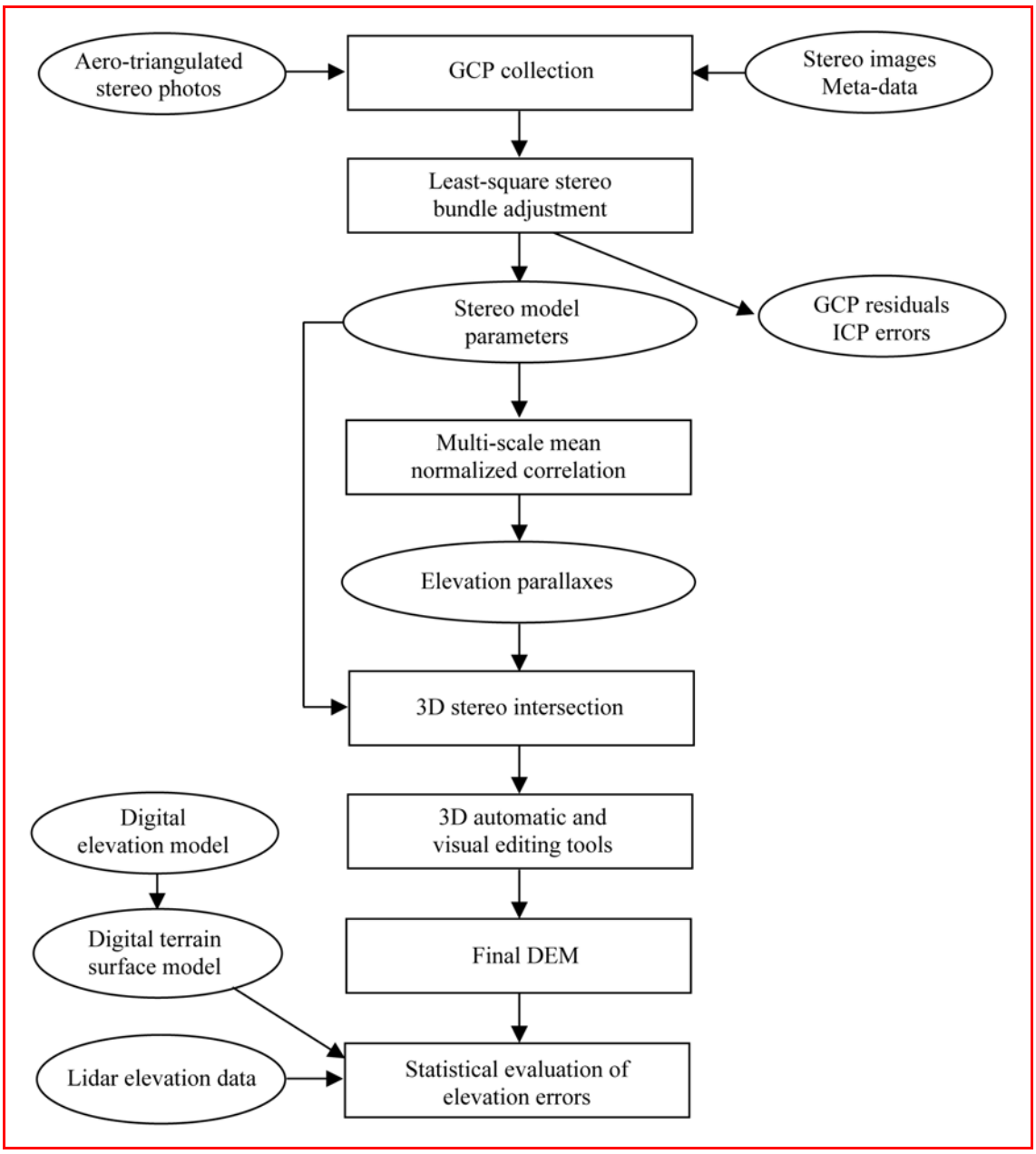

Figure 4. Processing steps for the DEM generation from stereo Ikonos images and its evaluation with lidar elevation data

The DEM is then evaluated with the lidar elevation data. About 5,500,000 points corresponding of the overlap area were used in the statistical computation of elevation errors. Different parameters (land cover and its surface height, terrain relief and slope), which have an impact on elevation errors, were also evaluated.

3 RESULTS AND DISCUSSIONS

Error propagation can be tracked along the processing steps with stereo bundle-adjustment results (Step 3), and during DEM generation (Steps 4 and 6). Even if the processing was performed on each stereo pair, only the quantitative results of the East stereo pair, where lidar elevation data was acquired, are given.

Stereo Bundle-Adjustment Results

As a function of numbers, location, and accuracies of GCPs used in the stereo bundle adjustment, four tests were performed: (#1) 30 GCPs; (#2) 10 GCPs and 20 ICPs, (#3) 30 GCPs including an erroneous GCP (which had a 20-m error in the *X*-direction); (#4) 10 GCPs and 20 ICPs, including an erroneous GCP (which had a 20-m error in the *X*-direction). Ten GCPs were used in Tests 2 and 4 because previous results demonstrated that it was a good compromise to maintain 1- to 2-m restitution accuracy with 1-m accurate GCP coordinates using a 3D physical model (Toutin, 2003). In addition, it enabled performance of an unbiased validation with ICPs, which were not used in the 3D stereo model calculation. Table 1 summarizes these results with the GCP residuals (root-mean-square (RMS) and maximum) (all tests), the RMS errors at ICPs (#2 and #4), and the residuals at the erroneous GCP (#3 and #4). When there are more GCPs than the minimum required for computing the stereo-model, the residuals mainly reflect the error of the input data, and the modeling accuracy is thus better (Toutin, 1995; Toutin, 2003). Consequently, it is thus normal and "safe" to obtain residuals from the least-squares adjustment in the same order of magnitude as the GCP error.

Table 1: Stereo bundle-adjustment results with the number of GCPs/ICPs for each test, the root-mean-square (RMS) residuals (in meters) and either minimum/maximum residuals (in meters) at the GCPs or the erroneous GCP residuals (in meters) or the RMS errors (in meters) at the ICPs.

Test Number	***X***	***Y***	***Z***	***X***	***Y***	***Z***
	RMS GCP Residuals			**Maximum Residuals**		
#1: 30 GCPs/0 ICP	1.9	1.8	2.2	5.3	3.5	6.6
	RMS GCP Residuals			**RMS ICP Errors**		
#2: 10 GCPs/20 ICPs	1.2	1.6	1.9	2.4	2.3	3.5
	RMS GCP Residuals			**Erroneous GCP Residuals**		
#3: 30 GCPs/0 ICP including 1 erroneous GCP	4.0	1.8	2.2	**17**	-1.0	0.5
	RMS GCP Residuals			**Erroneous GCP Residuals**		
#4: 10 GCPs/20 ICPs including 1 erroneous GCP	4.2	1.3	1.3	**14**	-1.5	3.2
				RMS ICP Errors		
				4.4	2.6	3.5

Table 1 shows that RMS residuals/errors (except #3 and #4) were generally in the same order of magnitude as the input error. In fact, the input error is a combination of image pointing error (1 to 2 m), *X*-*Y* planimetric error (1 m) and *Z*-error (2 m). The analysis of the *X*-*Y* maximum residuals for Test #1, which are generally around two to three times the RMS residuals, demonstrates that the 3D physical model is stable over the entire stereo images without generating local errors. Test #2 with ten GCPs confirmed this statement with the RMS errors on ICPs. However, these 2- to 3-m errors, which mainly include the extraction error of GCP features, are thus an estimation of the 3D restitution accuracy. The internal accuracy of the stereo model is in fact better, on the order of pixel or sub-pixel.

When an erroneous point was used as GCP (#3 and #4), the large residuals at this GCP when compared to the RMS residuals enabled the erroneous point to be easily detected. Furthermore, the direction and the approximate values of the error (20 m in the *X*-coordinate) were reflected in the erroneous GCP *X*-residual (17 m and 14 m for #3 and #4, respectively). The *X*-residual was larger when there were more GCPs (30 in #3 versus ten in #4) due to a larger degree of freedom in the least-squares stereo bundle adjustment. The use of overabundant GCPs in the least-squares stereo bundle adjustment (30 and even as few as ten) reduced the propagation of input data errors in the stereo-model, but conversely, these input errors are reflected in the GCP residuals. The RMS ICP *X* error (4.4 m in #4 versus 2.4 m in #2) demonstrates that a part of the erroneous GCP error propagated in the stereo model due to a reduced number of GCPs. Consequently, the model filtered random or systematic errors, and more GCPs enabled a better filtering. However, in any case, the error was detected.

Finally, since the RMS errors on ICPs and the RMS residuals on GCPs (#2 versus #1) were about the same order of magnitude as the input data errors, RMS residuals on GCPs can thus be used as *a priori* mapping error in operational environments, when taking into account the cartographic data errors. Similar results were obtained for the West stereo pair.

DEM Evaluation Results

The second result is the qualitative evaluation of the full DEM (2-m pixel spacing) extracted from the two stereo pairs and the quantitative evaluation of the DEM extracted from the East stereo pair. Plate 1 is a 3D chromostereoscopic representation of the full DEM, which well reproduces the terrain relief and different features of Figure 1. Specific features visible on the Ikonos images (Figures 1 and 2) are also identifiable on the DEM due to elevation differences: sand/gravel pits at A; some patterns at B related to streets/houses in residential areas, and linear features at C related to main roads and power-line clear-cut in the forest environment. In fact, the DEM is a digital surface model (DSM), which includes the heights of natural and human-made surfaces (trees, houses, hedges, etc.). As example, Figure 5 is a sub-area (1-m pixel

spacing, 512 pixels by 512 lines) of the stereo-extracted DEM (left) and of the Ikonos ortho image (right), where one can notice: (A) a deciduous forest without leaves, (B) a conifer forest, (C) groups or hedges of trees, (D) residential 1- and 2-story houses, (E) mobile homes, (F) residential streets, (G) a main street, and (H) a lake with its island. Consequently, a 3D visual classification on the stereo Ikonos images was performed to discriminate different classes: forests (deciduous, conifer, mixed, and sparse), residential, bare soil, and lakes. The rationale for the forest classification is that the Ikonos images were acquired in winter (deciduous without leaves) and the lidar data in summer (deciduous with leaves).

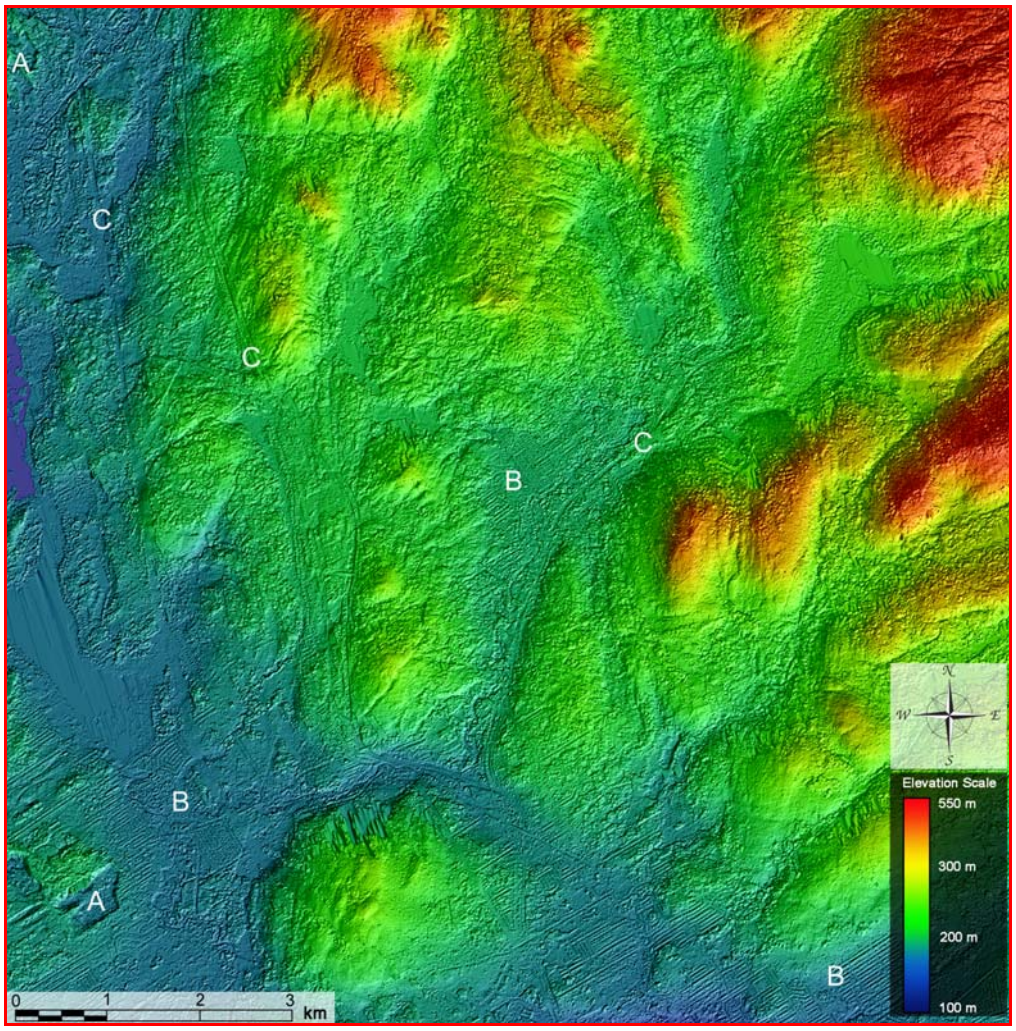

Plate 1. 3D chromostrereoscopic representation of the DEM (10 x 10 km; 1-m spacing) extracted from the two Ikonos stereo pairs. Lowest elevations (110 m) are in blue and highest (550 m) in red. (A) Sand pits, (B) Residential areas, (C) Roads and power lines. The linear features, which occur in residential areas (B) are not artifacts or systematic errors but are related to streets and houses patterns (see Figure 5).

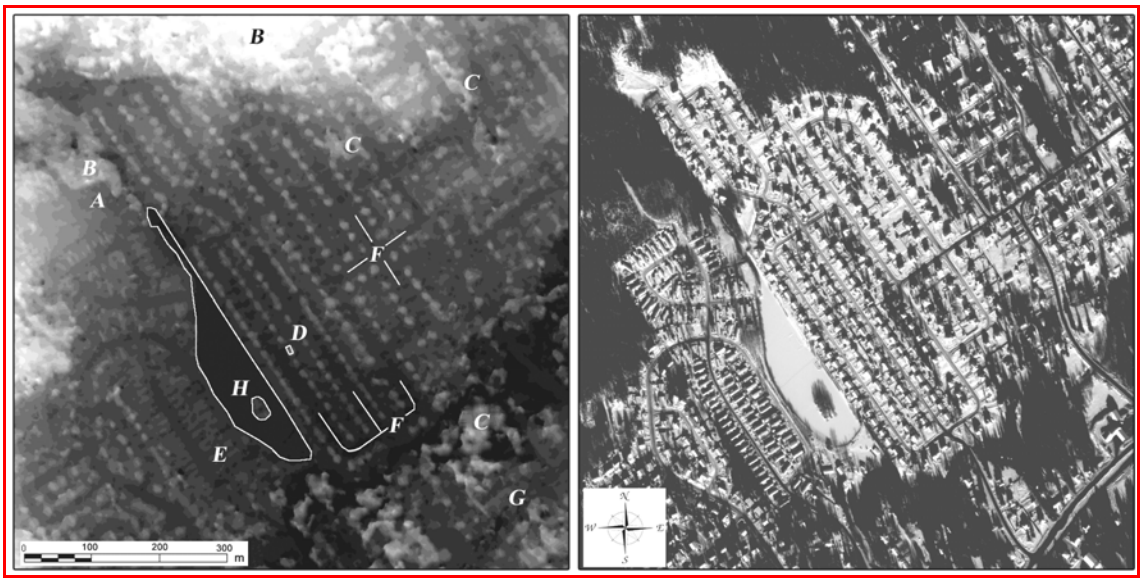

Figure 5. Sub-area (1-m pixel spacing, 512 pixels by 512 lines) of stereo extracted DEM (left) and of the Ikonos ortho image (right): (A) Deciduous forests without leaves, (B) conifer forests, (C) Groups or hedges of trees, (D) Residential 1- and 2-story houses, (E) Mobile homes, (F) Residential streets, (G) Main street, (H) Lake and its island. Ikonos Image © Space Imaging LLC, 2001.

The first quantitative evaluation was with the mismatched areas during the image matching. Even though the images were acquired in January with snow cover and frozen lakes, there are only 5 percent mismatched areas, of which includes 2.5 percent for lakes. The good matching performance over the lakes is due to the ice/snow and the tracks of the snowmobiles and skaters, creating texture and contrast (Figure 2). The remaining 2.5 percent mismatched areas are mainly located in the northwest slopes of mountains (Figure 2) due to the solar shadow (elevation angle of 19º and azimuth of 166º). These results confirm that multiscale matching performed well with 1 m high spatial resolution data in semirural areas due to a very good temporal resolution (a few seconds) with in-track stereo images. The East DEM was then compared with the lidar elevation data, and 5,500,000 points were used in the statistical computation.

Table 2 gives the statistical results computed from elevation errors: the linear errors at 68 percent and 90 percent levels of confidence (LE68 and LE90, respectively), the bias, and the percentage of the class over three times LE68 (in meters): the first line for the entire area of the East DEM and the other lines for the different land cover classes. The 6.4-m LE68 and 10-m LE90 with a 6-m bias for the entire area are medium results when compared to the stereo bundle adjustment results (2 to 3 m) but also in relation with the 1-m Ikonos pixel and a B/H of 1: the errors are mainly due to the canopy/building heights as mentioned previously (Figure 5). However, the largest errors (three times LE68), although they only represent less than 0.1 percent of the total,

are out of tolerance and cannot be acceptable for DEM in a topographic sense. In order to locate and understand these largest errors, they were superimposed on the DEM or on the Ikonos ortho image. They were mainly located in the mountains, trees, or buildings shadows (northwest direction) due to solar elevation and azimuth angles of 19º and 166º, respectively. Other large errors (15 to 20 m) result from the elevation comparison of the tops of trees versus the ground due to the different spatial resolutions of Ikonos and lidar data and to the different acquisition seasons. These errors are then representative of our stereo-images (acquired in winter) and experiment (lidar data acquired in summer), but they are not representative of the general Ikonos stereo performance for DEM generation.

Table 2. Statistical results from the comparison of stereo Ikonos DEM and lidar elevation data for the entire area of the East DEM and for the different land-cover classes: percentage of the entire area, linear error with 68 percent and 90 percent level of confidence (LE68 and LE90, respectively), bias, and percentage of the class over three times LE68. Best results (1.5-m LE68) were obtained over bare soil/lake areas.

Areas	Percentage	LE68	LE90	Bias	Over 3 LE68
Entire East DEM	100%	6.4 m	10 m	6 m	0.1%
Deciduous forests	31%	6.0 m	9 m	12 m	0.1%
Conifer forests	12%	4.0 m	7.5 m	2 m	2.4%
Mixed forests	36%	6.6 m	10 m	7 m	0.2%
Sparse forests	6%	4.0 m	8.5 m	4 m	4.3%
Urban/Residential	7%	2.5 m	6 m	4 m	6.7%
Bare soil/lakes	8%	**1.5 m**	**3.5 m**	**1 m**	5.0%

In fact, the results (Table 2) over bare soil/lakes (1.5-m LE68) better demonstrate the Ikonos stereo performance and the potential to generate 5-m contour lines with the highest topographic standard. This result was now more consistent with *a priori* 3D restitution accuracy from the stereo bundle adjustment (2 m in *Z*), and also reflected the potential Ikonos performance evaluation by Ridley *et al.* (1997) using simulated data. Better results could be thus expected when using stereo images acquired in summertime. For the residential class, the results are a little worse because 1- and 2-story houses (10 to 15 percent of the residential areas and 4 to 6 m in height, Figure 5) degrade the statistics a bit for this class. The results for the different forests are coherent with the nature of each class, taking into account the season variation between Ikonos images and lidar acquisitions and an estimation of tree heights (15 to 20 m and 10 to 15 m for the deciduous and conifers, respectively) in this study site:

1. For deciduous forests, the Ikonos elevation was approximately at the ground surface or higher while the lidar elevation was approximately at the top of the forest canopy: this elevation measurement variation was reflected in larger errors in LE68 and LE90, and mainly the 12-m bias.

2. For conifer forests, the Ikonos and lidar elevations were approximately representative of the same elevation, i.e., at top of the forest the canopy or a little lower: LE68, LE90, and bias were then much smaller and closer to the bare soil results.
3. For mixed forests, the Ikonos elevation can be either at the ground surface or at the top of the forest canopy, and the lidar elevation generally at the canopy top or a little lower: this non-homogeneous land-cover class normally gave the worse results for LE68 and LE90, but with a bias between the two previous forest-class biases (deciduous at 12 m and conifer at 2 m).
4. For sparse forests, the Ikonos and lidar elevations are similar to those for mixed forests but with much more values representative of the ground surface or a little higher: LE68, LE90, and bias are then much smaller, being similar to the conifer forest results and closer to the normally bare soil results.

These results for different land-cover classes explained the general results (6.4-m LE68) over the DEM because the two classes (deciduous and mixed) with the worst results (6-m and 6.6-m LE68, respectively) represent 67 percent of the DEM.

The next quantitative evaluations were related to the terrain relief (slopes and aspects). Figure 6 shows the statistical results (LE68 and LE90) with linear regression computed from a comparison of the elevations of the stereo-extracted DEM and the lidar data for each 1° slope class up to 25°. For slopes greater than 25°, there was not enough data in the classes to compute significant statistics.

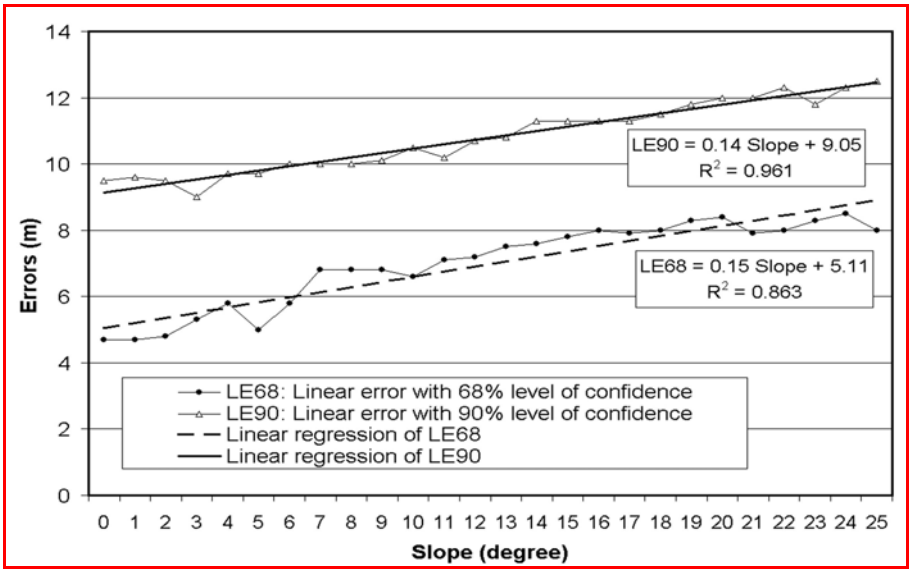

Figure 6. Statistical results (LE68 and LE90) with linear regression computed from a comparison of the elevations of the stereo-extracted DEM and the lidar data for each 1° slope bin up to 25°. At slopes greater than 25°, there is not enough data in the bins to compute significant statistics.

These slope results strongly enhanced for both LE68 and LE90 a linear correlation between elevation errors and slopes: the linear regression lines had the same gradient but with a stronger correlation factor for LE90 (0.961) than for LE68 (0.863). Finally, the error evaluation as a function of the slope azimuths showed that the LE68 in the sun-facing slopes (azimuths from 76º to 256º) was only 1-m smaller than the LE68 in the slopes away from the sun (azimuths from 256º to 76º). Even if most of the largest errors were in the slopes away from sun, less than 2 percent of the total slopes generated shadows due to terrain relief, which explained the small difference in LE68.

4 CONCLUSIONS

A DEM was extracted from in-track Ikonos stereo images (B/H of 1) acquired over a residential/rural hilly area in Quebec, Canada, and using the CCRS 3D physical model and multiscale image matching. The 3D physical model enabled input errors to be detected and filtered and the stereo bundle adjustment using ten GCPs enabled *a priori* 3D restitution accuracy to be estimated (around 2 to 3 m in the three axes). The stereo-extracted DEM was then compared to accurate elevation lidar checked data, and an elevation error of 6.4 m (LE68) was obtained. The largest errors (over 15 m) occurred in areas shadowed due to mountains, trees, and buildings, but were also due to the elevation comparison between winter-acquired stereo images (no leaves on deciduous trees) and summer-acquired lidar check data (leaves on deciduous trees). Because the surface heights were included in terrain elevation, the elevation errors were also evaluated as a function of the land cover (bare surfaces; urban areas; deciduous, conifer, mixed and sparse forests). The worse results (6.0- to 6.6-m LE68) were obtained over deciduous and mixed forests, resulting from the different seasons between the Ikonos image and lidar data acquisitions. The best results (1.5-m LE68), which were obtained on bare surfaces where there was no elevation difference between the stereo DEM and lidar data, are a good indication of the general Ikonos stereo performance for DEM generation. While elevation errors were linearly correlated with the terrain slopes, slope aspects did not have too much affect on elevation errors (LE68 and LE90), but did affect the largest errors, which occur on the slopes away from sun. Because these errors are specific to this data set, better results could be expected with stereo pairs acquired in summertime.

Acknowledgements

The author thanks Mr. Réjean Matte of the Ministère des Ressources naturelles du Québec, Canada for the topographic data and GPR Consultants for the lidar survey. He also thanks M. René Chénier and M. Yves Carbonneau of Consultants TGIS inc., Canada for processing the data.

References

Fowler, R.A., 2001. The Thorny Problem of Lidar Specifications, *Earth Observation Magazine*, 10(4):13-17, URL: http://www.lasermap.com/laserM/english/princ.htm, last accessed 05 March 2004.

Fraser, C.S., E. Baltsavias, and A. Gruen, 2002. Processing of Ikonos imagery for submetre 3D positioning and building extraction, *ISPRS Journal of Photogrammetric Engineering and Remote Sensing*, 56(3):177-194.

Fritz, L.W., 1996. The era of commercial Earth observation satellites, *Photogrammetric Engineering & Remote Sensing*, 62(1):39-45.

Gülch, E., 1991. Results of Test on Image Matching of ISPRS WG III/4, *ISPRS Journal of Photogrammetry and Remote Sensing*, 46(1):1-8.

Kaufmann, V., und W. Sulzer, 1997. Über die Nutzungsmöglichkeit hochauflösender amerikanischer Spionage-Satellitenbilder (1960-1972), *Vermessung und Geoinformation*, Heft 3/97:166-173.

Konecny, G., 2000. Mapping from Space, *Remote Sensing for Environmental Data in Albania: A Strategy for Integrated Management, Tirana, Albania* (M. F. Buchroithner, editor), NATO Science Series, Vol. 72, Kluwer Academic Publishers, Dordrecht, The Netherlands, pp. 41-58.

Leberl, F., 1998. Radargrammetry, *Manual of Remote Sensing* (F. M. Henderson and A. J. Lewis, editors), John Wiley & Sons, Inc., New York, N.Y., pp. 183-269.

Li, R., 1998. Potential of high-resolution satellite imagery for national mapping product, *Photogrammetric Engineering & Remote Sensing*, 64(12):1165-1170.

Madsen, S. N., and H.A. Zebker, 1998. Imaging radar interferometry, *Manual of Remote Sensing* (F. M. Henderson and A. J. Lewis, editors), John Wiley & Sons, Inc., New York, N.Y., pp. 359-380.

Muller, J.-P., J.-R. Kim and L. Tong, 2001. Automated mapping of surface roughness and landuse from simulated and spaceborne 1m data, *Automatic Extraction of Man-Made Objects From Aerial and Space Images (III)* (E. P. Baltsavias, A. Gruen, and L. van Gool, editors), A.A. Balkema, Rotterdam, The Netherlands, pp. 369-379.

Ridley, H.M., P.M. Atkinson, P. Aplin, J.-P. Muller, and I. Dowman, 1997. Evaluating the potential of the forthcoming commercial U.S. high-resolution satellite sensor

imagery at the Ordnance Survey®, *Photogrammetric Engineering & Remote Sensing*, 63(8):997-1005.

Tao, C.V., and Y. Hu, 2002. 3D reconstruction methods based on the rational function model, *Photogrammetric Engineering & Remote Sensing*, 68(7):705-714.

Toutin, Th., 1995. Generating DEM from Stereo-Images with a Photogrammetric Approach: Examples with VIR and SAR data, *EARSeL Advances in Remote Sensing*, 4(2): 110-117, URL: http://www.ccrs.nrcan.gc.ca/ccrs/rd/sci_pub/bibpdf/13150.pdf, last accessed 05 March 2004.

Toutin, Th., 2000. Elevation modeling from satellite data, *Encyclopedia of Analytical Chemistry: Applications, Theory and Instrumentation* (R. A. Meyers, editor), Vol. 10, John Wiley & Sons, Ltd., Chichester, United Kingdom, pp. 8543-8572, URL: http://www.ccrs.nrcan.gc.ca/ccrs/rd/sci_pub/bibpdf/4622.pdf, last accessed 05 March 2004.

Toutin, Th., 2003. Error tracking in Ikonos geometric processing using a 3D parametric modeling, *Photogrammetric Engineering & Remote Sensing*, 69(1):43-51, URL: http://www.ccrs.nrcan.gc.ca/ccrs/rd/sci_pub/bibpdf/13102.pdf, last accessed 06 February 2004.

Toutin, Th., and P. Cheng, 2001. DEM with Stereo IKONOS: A Reality if…, *Earth Observation Magazine*, 10(7):13-17, URL: http://www.ccrs.nrcan.gc.ca/ccrs/rd/sci_pub/bibpdf/13113.pdf, last accessed 05 March 2004.

Toutin, Th., R. Chénier, and Y. Carbonneau, 2001. 3D Geometric modelling of IKONOS Geo images, *Proceedings of the ISPRS Joint Workshop "High Resolution Mapping from Space,"* 19-21 September, Hannover, Germany, CD-ROM, pp. 272-280, URL: http://www.ccrs.nrcan.gc.ca/ccrs/rd/sci_pub/bibpdf/13117.pdf, last accessed 05 March 2004.

(Received 31 July 2002; accepted 16 April 2003; revised 23 June 2003)